



Synthesis and characterization of the functionalized nanoparticle and dye removal modeling

Niyaz Mohammad Mahmoodi*, Javad Abdi, Zahra Afshar-Bakeshloo, Jafar Abdi

Department of Environmental Research, Institute for Color Science and Technology, Tehran 1668814811, Iran,

Tel. +98 021 22969771; Fax: +98 021 22947537; emails: mahmoodi@icrc.ac.ir, nm_mahmoodi@aut.ac.ir, nm_mahmoodi@yahoo.com

(N.M. Mahmoodi), javad9524@gmail.com (J. Abdi), zarzar.afshar111@yahoo.com (Z. Afshar-Bakeshloo), jafar.abdi1989@gmail.com

(J. Abdi)

Received 27 April 2015; Accepted 11 December 2015

ABSTRACT

In this paper, copper oxide nanoparticle was synthesized and its surface was functionalized to remove dyes from single systems. The characteristics of the adsorbent were studied using Fourier transform infrared, X-ray diffraction, and scanning electron microscopy. Direct Red 31 (DR31) and Direct Red 80 (DR80) were used as model dyes. Least-squares support vector machine was used to predict dye removal. The model shows better performance in predicting dye removal compared to the kinetic models with average absolute percent relative error of 3.278 and 3.787% for DR31 and DR80, respectively, and correlation coefficients close to unity. Therefore, the used model could be reliable for prediction of the dye removal efficiency.

Keywords: Synthesis; Functionalized nanoparticle; Characterization; Dye removal modeling; Single system

1. Introduction

It is necessary to investigate pollutants in aquatic samples, because many of these compounds can pose threats to human health and the ecosystem. Dye removal from colored wastewater has been a major concern of different industries, especially for textile industry. Therefore, their removals from industrial effluents before discharge into the environment require extreme and great attention. Several methods such as physical, biological, photocatalysis, electrochemical, etc. have been used to remove organic pollutants from wastewater [1–6]. Each method has its advantages and disadvantages. For example, ozonation suffers from high operating costs. Biological treatment methods are

ineffective for degradation due to the large degree of aromatics present in dye molecules and the stability of modern dyes [3]. Organic compounds such as dyes, sericin, etc. can be degraded by enzymes [7,8]. Filtration potentially provides pure water but low molar mass dyes can pass through the filter system [3].

Adsorption process is one of the physical wastewater treatment processes. It is considered to be relatively superior to other techniques due to low cost, simplicity of design, availability and ability to treat dyes in more concentrated form [9,10].

A literature review showed that the functionalized copper oxide nanoparticle (CuO-NH₂) was not investigated to adsorb anionic dyes from wastewater. In this paper, copper oxide nanoparticle (CuO) was synthesized and functionalized using (3-aminopropyl) trimethoxy silane. The characteristics of CuO-NH₂

*Corresponding author.

were investigated using Fourier transform infrared (FTIR), X-ray diffraction (XRD), and scanning electron microscopy (SEM). Direct Red 31 (DR31) and Direct Red 80 (DR80) were used as model dyes. The dependency of adsorption performances to effective variables such as contact time, adsorbent dosage, initial dye concentration, and pH was systematically studied. To obtain the best control and management, new concepts including effective operation and design should be improved and comprehended. Hence, a high quality representative model can supply a desirable solution in the process control and helps to illustrate the real process performance and to develop a continual control strategy for this kind of technologies. The models such as least square supported vector machine (LSSVM) have many adjustable parameters containing of weights and biases [11]. In this work, LSSVM was used to predict the dye removal efficiency of single system based on the obtained laboratory data under different experimental conditions. To improve this model, 220 data-sets have been utilized from dye removal experimental tests. In addition, dye adsorption isotherm and kinetics was studied.

2. Experimental

2.1. Materials

Direct Red 31 (DR31) and Direct Red 80 (DR80) were used. The dye solutions were prepared by dissolving a defined quantity of the dye in distilled water. The characteristics of the dyes are shown in Table 1. All other chemicals were of analytical grade and purchased from Merck (Germany).

2.2. Synthesis of CuO-NH₂

2.2.1. Synthesis of CuO

0.25 g of CuSO₄·5H₂O and 0.4 g of NaOH were dissolved under stirring in 30 mL of distilled water. The mixed solution was sealed in a glass bottle and kept static at 120°C for 24 h, and then cooled to room temperature naturally. The final precipitate was washed with distilled water several times to remove the possible residues and then dried at 120°C for 12 h [12].

2.2.2. Synthesis of CuO-NH₂

One gram of CuO and 1 g of (3-aminopropyl) trimethoxy silane were poured into mixture of water and ethanol and mixed for 24 h at 25°C. The precipitate was filtered, washed with deionized water, and dried.

2.3. Adsorption procedure

The dye adsorption measurements were done by mixing various adsorbent dosages (0.05–0.4 g) of dyes in jars containing 250 mL of a dye solution (50 mg/L). Dye solutions were prepared using distilled water to prevent and minimize possible interferences. Experiments were carried out at 25°C for 60 min to attain equilibrium conditions. After experiments, the adsorbent was separated from solution samples and then the dye concentration was determined. The changes of absorbance were determined at certain time intervals (2.5, 5, 7.5, 10, 15, 20, 30, 40, 50, and 60 min) during the adsorption process using UV-vis Perkin-Elmer Lambda 25 spectrophotometer. The maximum wavelength (λ_{\max}) of DR31 and DR80 to determine residual dye concentration in solution was 523 and 543 nm, respectively.

The effect of adsorbent dosage (0.0125–0.1000 g) on dye removal was investigated by contacting 250 mL of dye solution with initial dye concentration of 50 mg/L at room temperature (25°C) for 60 min and pH 2.1.

The effect of initial dye concentration (50, 100, 150, and 200 mg/L) on dye removal was investigated by contacting 250 mL of dye solution with adsorbent at room temperature (25°C) for 60 min and pH 2.1.

The effect of pH (2.1, 5, 8, and 10) on dye removal was investigated by contacting 250 mL of dye solution with adsorbent and initial dye concentration (50 mg/L) at room temperature (25°C) for 60 min.

2.4. Adsorbent characterization

The functional groups of the material were studied using FTIR spectroscopy (Perkin-Elmer Spectrophotometer Spectrum One) in the range of 4,000–450 cm⁻¹. Crystallization behavior was identified by XRD model Siemens D-5000 diffractometer with Cu K_α radiation ($\lambda = 1.5406 \text{ \AA}$) at room temperature. The morphological structure of the material was examined by SEM using a LEO 1455VP scanning microscope.

3. Modeling theory

3.1. Data-set and software

To improve the LSSVM model, 220 data-sets have been used from dye removal experimental tests for single system. Parameters of adsorbate type, adsorbent dosage, dye concentration, pH, and contact time were used as inputs to LSSVM model to predict equilibrium adsorption (i.e. output). Table 2 summarizes the input/output variables of the model as well as their domains. As it can be seen, employed data bank

Table 1
Chemical structure and characteristics of dyes

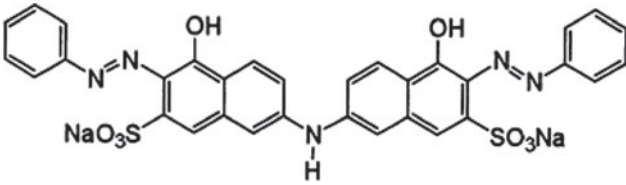
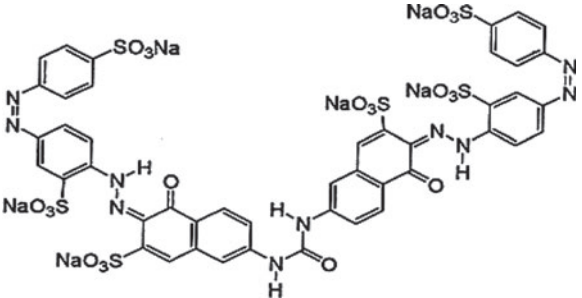
Chemical name	Chemical structure	Color index number	λ_{\max} (nm)	M_w (g/mol)
Direct Red 31	 $C_{32}H_{21}N_5Na_2O_8S_2$	13,390	523	713.6
Direct Red 80	 $C_{45}H_{26}N_{10}Na_6O_{21}S_6$	35,780	543	1373.1

Table 2
Ranges of the data were used for developed models

	Variable	Range/Type
Input	Adsorbate type	DR31, DR80
	Adsorbent dosage	0.05–0.4 g/L
	Dye Concentration	0.05–0.2 g/L
	Initial pH	2.1–10
	Contact time	0–60 min
Output	Equilibrium adsorption	0–6.2 (mg/g)

covers a wide range of experimental conditions. The free LSSVM toolbox (LSSVM V-1.8, Suykens, Leuven, Belgium) was applied with MATLAB Version R2010b to gather all the LSSVM models.

3.2. Model development

The aim of this study is to develop nonlinear relationships between the available experimental data regarded as inputs of the model (adsorbent dosage, dye concentration, pH, and contact time), and the desired output (Equilibrium adsorption). For this purpose, an appropriate mathematical tool is required. The support vector machine (SVM) has been considered as a powerful strategy improved from the

machine-learning community [11,13,14]. The SVM has been studied widely for both classification and regression analysis and it is regarded as a non-probabilistic binary linear classifier [15–17]. It plans the input patterns into a higher dimensional feature space through non-linear mapping function i.e. kernel function. A linear decision surface is then built to relate the original input space to output variables [17]. Some advantages of the SVM-based methods over the traditional methods based on the ANNs are as follows [11]:

- (1) The possibility of model convergence is higher in the SVM-based methods.
- (2) Normally, SVM-based methods apply standard and straightforward algorithms.
- (3) The topology of the network in the SVM-based methods is appointed after completion of the training stage.
- (4) There is no need to select the number of hidden nodes- hidden layers.
- (5) Generalization performance is satisfactory in SVM-based methods.
- (6) There are usually two adjustable parameters required. This is generally less than that required for other ANN methods.

In spite of these advantages, SVM-based methods have some disadvantages [18]:

- (1) Perhaps the biggest limitation of the support vector approach lies in choice of the kernel.
- (2) A second limitation is speed and size, both in training and testing.
- (3) Discrete data presents another problem.
- (4) The optimal design for multiclass SVM classifiers is a further area for research.

A modified version of SVM, namely; Least Squares SVM was suggested by Suykens and Vandewalle [11] to decline the SVM complexity. The LSSVM method takes useful advantages of SVM. Besides, it needs solving a set of linear (relative to nonlinear) equations, resulting in a swifter and more feasible alternative to the traditional SVM method.

The regression error of the LSSVM approach is defined as the difference between the represented and predicted property values and experimental ones, which is regarded as an addition to the constraint of the optimization problem [11,19]. In most prevalently used SVM method, the value of the regression error is normally optimized during the calculations while in the LSSVM it is mathematically defined [11,19,20]. The penalized cost function of the applied LSSVM model is determined as below [11,21,22]:

$$Q_{\text{LSSVM}} = \frac{1}{2} w^T w + \gamma \sum_{i=1}^N e_i^2 \quad (1)$$

$$y_i = w^T \varphi(x_i) + b + e_i \quad i = 1, 2, \dots, N \quad (2)$$

where w shows the regression weight (slope of the linear regression), e_i displays the regression error for N training objects, and γ hints the relative weight of total regression errors compared to the regression weight. Moreover, φ represents the feature map, in which the experimental data can be linearly separated by a hyper plane specified by the pair $(w \in R^m, b \in R)$ [19,21,22]. The weight coefficient (w) is usually written as follows [17,19]:

$$w = \sum_{i=1}^N \alpha_i x_i \quad (3)$$

In which:

$$\alpha_i = 2\gamma e_i \quad (4)$$

By applying the fundamentals of the LSSVM algorithm, Eq. (2) is re-written as follows [17,19]:

$$y = \sum_{i=1}^N \alpha_i x_i^T x + b \quad (5)$$

Therefore, the Lagrange multipliers (α_i) are calculated as [17,19]:

$$\alpha_i = \frac{(y_i - b)}{x_i^T x + (2\gamma)^{-1}} \quad (6)$$

The above-mentioned linear regression equation could be retreated as nonlinear one by using the Kernel function as follows [17,19]:

$$f(x) = \sum_{i=1}^N \alpha_i K(x, x_i) + b \quad (7)$$

where $K(x, x_i)$ is the Kernel function calculated from the inner product of the two vectors x and x_i in the feasible region built by the inner product of the vectors $\Phi(x)$ and $\Phi(x_i)$ as follows [21,22]:

$$K(x, x_i) = \Phi(x)^T \cdot \Phi(x_i) \quad (8)$$

The radial basis function (RBF) Kernel is the most common function that has been utilized as below [21,22]:

$$K(x, x_i) = \exp\left(\frac{-\|x_i - x\|^2}{\sigma^2}\right) \quad (9)$$

where σ is regarded to be a decision variable, which is optimized by an external optimization algorithm during the calculations [19,22]. The mean square error (MSE) of the results of the LSSVM [14] algorithm has been defined by the following equation:

$$\text{MSE} = \frac{\sum_{i=1}^n (E_{\text{pred},i} - E_{\text{exp},i})^2}{n} \quad (10)$$

where $E_{\text{pred},i}$ is the predicted value by presented model, $E_{\text{exp},i}$ is the experimental value, and n is the number of samples from the initial population. The LSSVM algorithm was applied in this study to train the dye removal efficiency data as carried out by other researchers [11].

3.3. Computational procedure

In order to make uniform the domain of variables, each data were mapped into range $(-1, 1)$ by the following equation:

$$x_n = 2 \times \frac{(x - x_{\min})}{(x_{\max} - x_{\min})} - 1 \quad (11)$$

where x and x_n are original and normalized values of the desired variable, respectively. While, x_{\min} and x_{\max} are extreme values of the variable. In order to calculate the statistical errors of the developed models, all of the prediction values (i.e. outputs of the network) were performed an inverse range scaling to bring the predicted values to their original scales. This preprocessing procedure has been applied to obtain the parameters of the LSSVM algorithm. Later, these values were changed to their original values. In the next step, the database was divided into three sub-data sets including the training set, validation set, and the test set. Generally, the training set is used to generate the model structure, and the test set is used to investigate the prediction capability and validity of the proposed model [14,22]. The division of database into three sub-data sets is normally performed randomly. For this purpose, 70, 15, and 15% of the main data-set were randomly selected for building the LSSVM models (i.e. training set), check the validation and test, respectively.

4. Results and discussion

4.1. Characterization

The FT-IR spectrum of CuO nanoparticle was shown in Fig. 1. It has two peaks at 3,450 and 600–500 cm^{-1} which indicate O–H stretching vibration and metal-oxygen vibration, respectively [23]. The peak at 1,625 cm^{-1} was attributed to OH bending of

molecular water [24]. The FTIR spectrum of the surface functionalized nanoparticle (CuO-NH₂) displays a number of characteristic bands at 3,403, 2,920, and 600–500 cm^{-1} (Fig. 1). These bands are assigned to O–H and N–H stretching vibration, –CH₂– vibration, and metal-oxygen vibration, respectively [24]. The bending vibration of N–H (amine) and C–N (amine) display a strong band at 1,600–1,560 cm^{-1} and 1,350–1,000 cm^{-1} , respectively [23].

Fig. 2 illustrates the XRD pattern of the CuO nanoparticle. All diffraction peaks in Fig. 2 are in good agreement with those of the standard pattern of monoclinic CuO (JCPDS Card No. 05-0661). The Miller indices matched well with the reflections of the CuO nanoparticle reported in the previous published paper [12].

SEM is used to determine the particle shape and appropriate size distribution of the material. The SEM micrograph of the CuO nanoparticle and the functionalized CuO nanoparticle (Fig. 3) shows a relatively homogeneous nanoparticle size distribution.

4.2. LSSVM modeling

Generally, there are two important parameters in the LSSVM algorithm i.e. σ^2 and γ , that must be calculated before model development. These parameters were evaluated using Coupled Simulated Annealing (CSA) optimization technique [25]. The optimization procedure was repeated for several times as tries to arrive to the most probable global optimum of the objective function. Squared decision variable (σ^2) is computed using external optimization algorithm as 2.946 and 5.277 for DR31 and DR80, respectively.

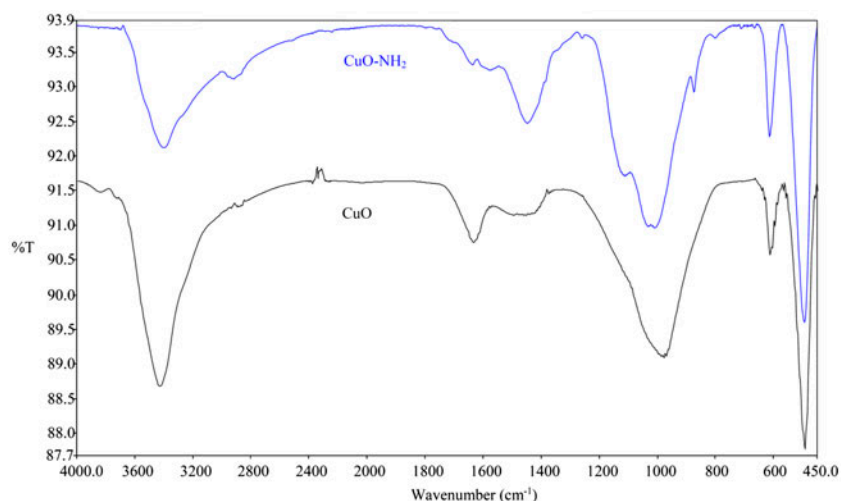


Fig. 1. FT-IR spectrum of the synthesized particles.

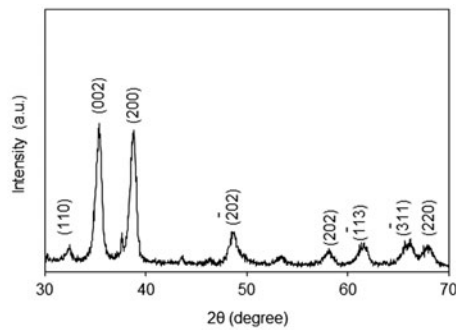


Fig. 2. XRD pattern of CuO nanoparticle.

The relative weights of total regression errors compared to the regression weight were also evaluated as $\gamma = 3.128e + 05$ and $\gamma = 1.009e + 05$ for DR31 and DR80, respectively.

A comparison between the prediction of the expert model and the corresponding experimental equilibrium adsorption data for DR31 and DR80 are illustrated in Fig. 4. Closely distributed data points around 45° line for training, validation, and testing data demonstrates the appropriateness of the developed LSSVM model in this regard [11]. In addition, it is evident that proposed LSSVM model has the small error range and least scatter around zero error line (Fig. 5).

Fig. 6 indicates absolute relative errors of the datasets. It is clear from Fig. 6 that the maximum error is less than 15% and the average one is near 3.5%. These values are reasonable from statistical point of view.

Furthermore, some important statistical parameters of the proposed model including average relative deviation, average absolute relative deviation, standard deviation error, squared correlation coefficient (R^2), and root MSE are reported in Table 3. APRE and AAPRE error values confirm that the relative deviation of the expert model from the experimental data is negligible. Moreover, RMSE, STD, and R^2 indicate highly acceptable agreement of the developed model with the actual data. The results indicate that an excellent accordance exists between the expert model predictions and the experimental data and obviously, confirm that LSSVM model reproduce the decolorization efficiency in our system, within the experimental ranges used in the model fitting.

4.3. Effect of CuO-NH₂ dosage

The physical removal of direct dyes in aqueous solution with various CuO-NH₂ dosages was studied. The experimental and LSSVM calculated values of removal are shown in Fig. 7. The increase in dye

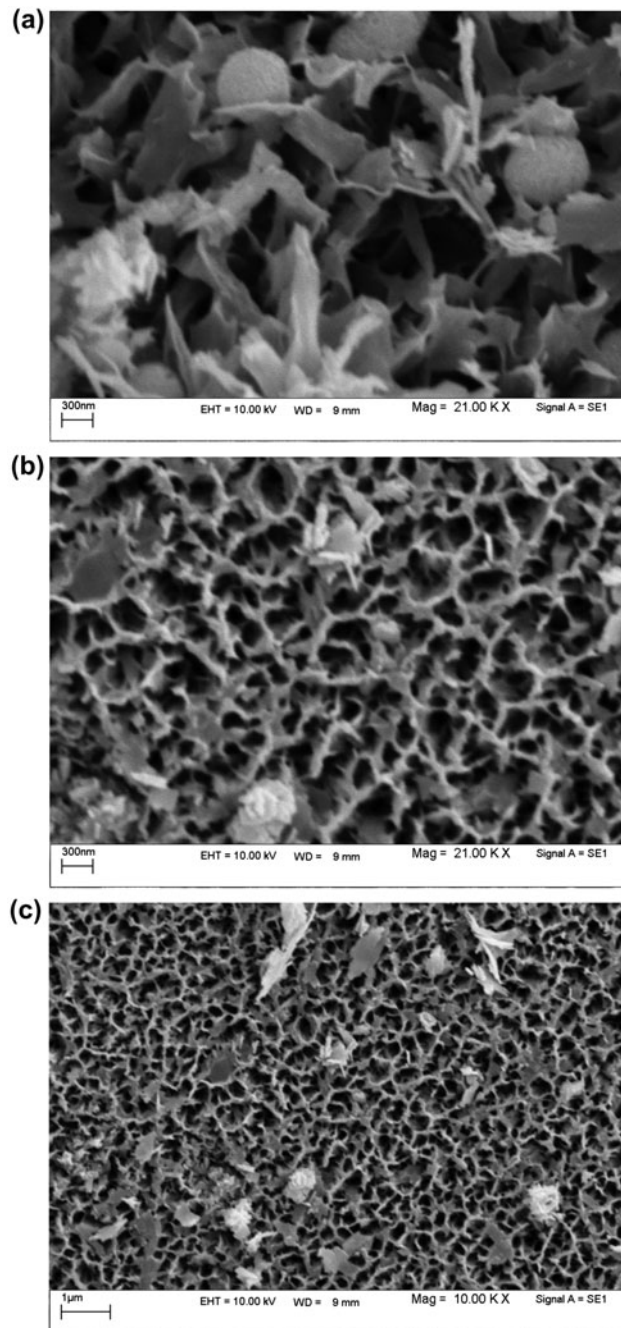


Fig. 3. SEM images of the synthesized nanoparticles (a) CuO and (b and c) CuO-NH₂.

removal with adsorbent dosage can be attributed to the increasing of adsorbent surface and availability of more adsorption sites. However, if the adsorption capacity was expressed in mg adsorbed per gram of material, the capacity decreased with the increasing amount of adsorbent. The comparison between LSSVM and experimental data in Fig. 7 shows that the results are in good agreement.

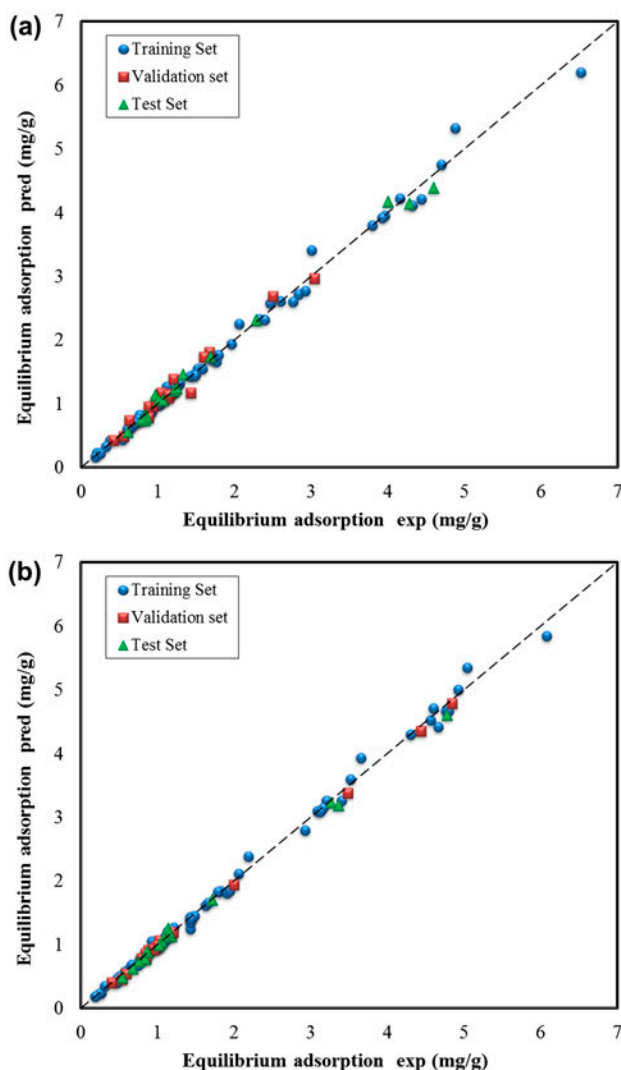


Fig. 4. Comparison between predicted results of the developed model and experimental data: (a) DR31 and (b) DR80.

4.4. Effect of initial dye concentration

The effect of initial dye concentration on the dye removal efficiency was analyzed over a dye concentration range from 50 to 200 mg/L (Fig. 8). The results showed that the higher the initial dye concentration, the lower the percentage of dye adsorbed. The amount of the dye adsorbed onto adsorbent increases with an increase in the initial dye concentration of solution if the amount of adsorbent is kept unchanged due to the increase in the driving force of the concentration gradient with the higher initial dye concentration. At a fixed adsorbent dosage, the amount of dye adsorbed increased with increasing concentration of solution, but the percentage of adsorption decreased. In other words, the residual dye concentration will be higher

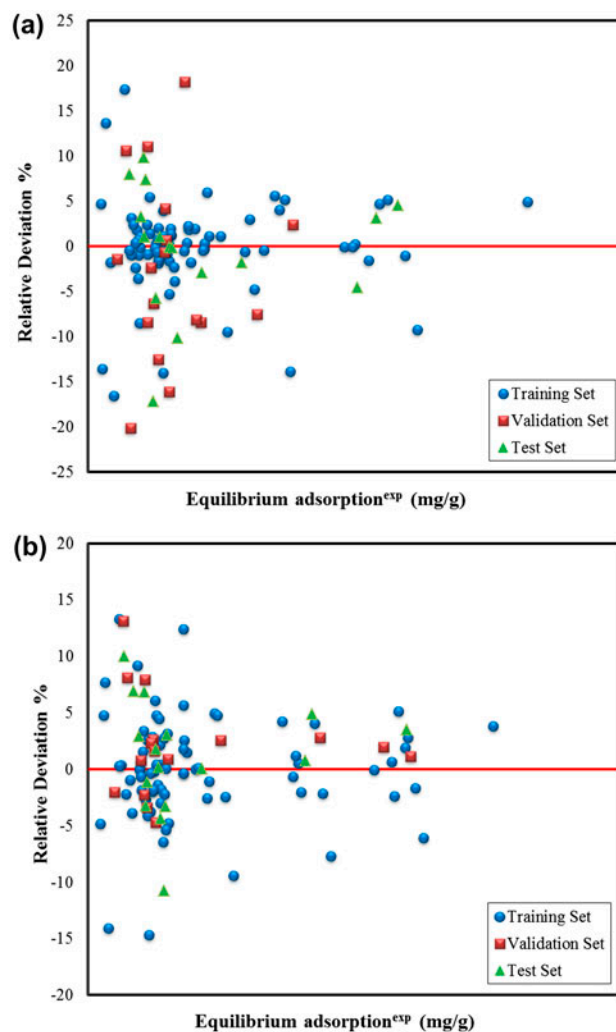


Fig. 5. Relative deviations of the determined equilibrium adsorption values from experimental ones by the developed model: (a) DR31 and (b) DR80.

for higher initial dye concentrations. The results confirm that the LSSVM model could effectively reproduce the experimental results for dyes.

4.5. Effect of pH

Fig. 9 shows the dye removal efficiency as a function of pH. The adsorption capacity increases when the pH is decreased. Maximum adsorption of anionic dyes occurs at acidic pH (pH 2.1). The electrostatic attraction as well as the organic property and structure of dye molecules and adsorbent could play very important roles in dye adsorption on adsorbent. At pH 2.1, a significantly high electrostatic attraction exists between the positively charged surface of the adsorbent, due to the ionization of functional groups of adsorbent and

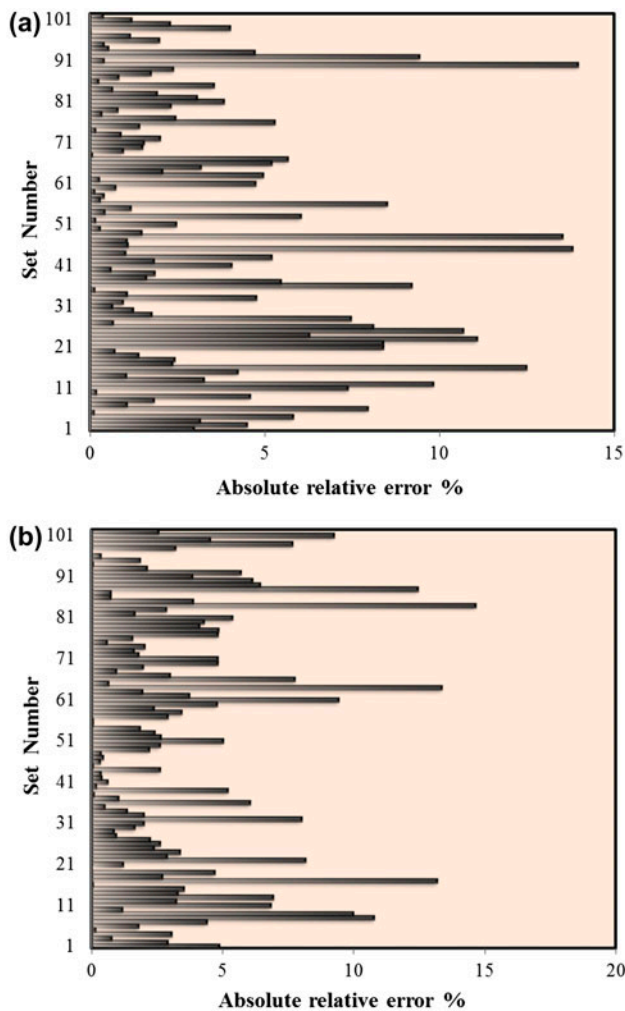


Fig. 6. Absolute relative error percentage of the obtained results from the corresponding experimental values: (a) DR31 and (b) DR80.

negatively charged anionic dye. As the pH of the system increases, the number of positively charged sites decreased. It does not favor the adsorption of anionic dyes due to the electrostatic repulsion [26]. The effective pH was 2.1 and it was used in further studies. The comparison between prediction model of LSSVM and experimental data in Fig. 9 shows that the results are in superior agreement.

4.6. Adsorption isotherm

The mechanism of dye removal was investigated by isotherm models. Several isotherms such as the Langmuir, Freundlich, and Tempkin models were studied in details [27–30].

The Langmuir isotherm explains the adsorption of dye on adsorbent. A basic assumption of the Langmuir theory is that adsorption takes place at specific sites on the adsorbent surface [31–34]. The Langmuir equation is as follows:

$$C_e/q_e = (1/K_L Q_0) + C_e/Q_0 \quad (12)$$

where q_e , C_e , K_L , and Q_0 are the amount of dye adsorbed at equilibrium (mg/g), the equilibrium concentration of dye in solution (mg/L), the Langmuir constant (L/g), and the maximum adsorption capacity (mg/g), respectively.

The Freundlich isotherm is as [35]:

$$\log q_e = \log K_F + (1/n) \log C_e \quad (13)$$

where K_F is adsorption capacity at unit concentration and $1/n$ is adsorption intensity.

Table 3

Statistical parameters of the developed LSSVM model to determine equilibrium adsorption

	Set	N^a	APRE (%)	AAPRE (%)	RMSE	STD	R^2
DR31	Training	77	-0.120	3.169	0.100	0.152	0.994
	Validation	17	-2.607	8.170	0.119	0.167	0.971
	Prediction	16	-0.299	5.058	0.101	0.330	0.994
	Total	110	-0.271	3.278	0.099	0.165	0.994
DR80	Training	77	0.046	2.640	0.081	0.179	0.997
	Validation	17	1.036	5.982	0.084	0.325	0.996
	Prediction	16	1.124	4.541	0.091	0.234	0.995
	Total	110	0.166	3.787	0.082	0.153	0.997

^aNumber of experimental data points.

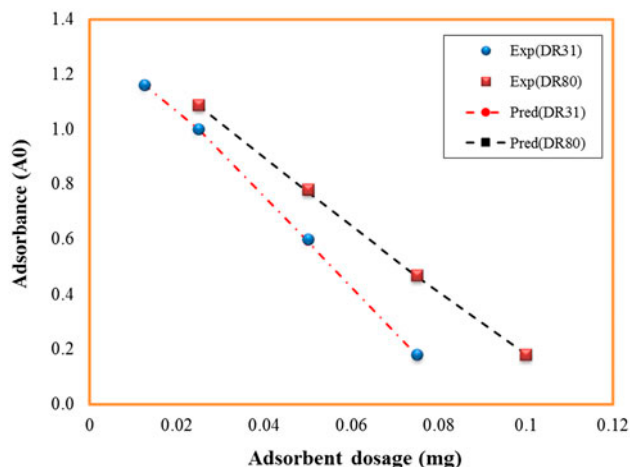


Fig. 7. Comparison between LSSVM-predicted and experimental values of equilibrium absorbance as a function of initial amount CuO-NH₂ at the time of 60 min: pH 2.1, [Dye]_o = 50 mg/L.

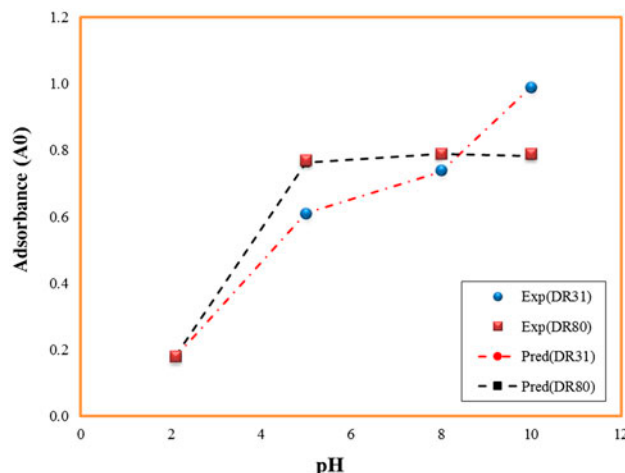


Fig. 9. Comparison between LSSVM-predicted and experimental values of equilibrium absorbance as a function of pH at the time of 60 min: [Dye]_o = 50 mg/l and [CuO-NH₂] = 0.3 g/L for DR31 and [CuO-NH₂] = 0.4 g/L for DR80.

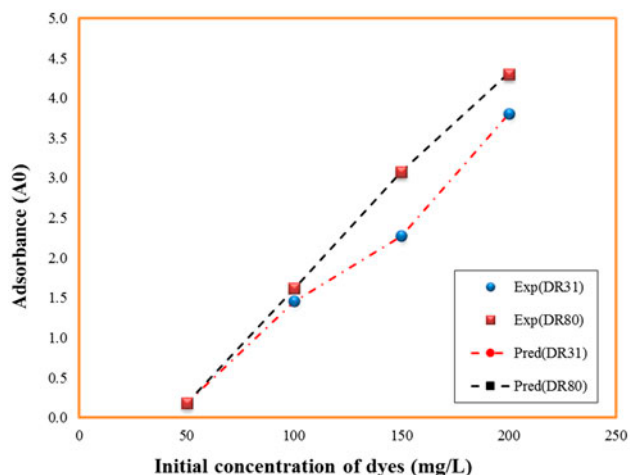


Fig. 8. Comparison between LSSVM-predicted and experimental values of equilibrium absorbance as a function of initial dye concentration at the time of 60 min: pH 2.1 and [CuO-NH₂] = 0.3 g/L for DR31 and [CuO-NH₂] = 0.4 g/L for DR80.

The Tempkin isotherm is given as [36]:

$$q_e = B_1 \ln K_T + B_1 \ln C_e \tag{14}$$

where K_T is the equilibrium binding constant (L/mg) corresponding to the maximum binding energy and the constant B_1 (RT/b) is related to the heat of adsorption.

The parameter values related to Langmuir, Freundlich, and Tempkin isotherms were calculated

from the slope and intercept of the plots (C_e/q_e vs. C_e), ($\log q_e$ vs. $\log C_e$), and (q_e vs. $\ln C_e$), respectively. The values of Q_0 , K_L , K_F , n , K_T , B_1 , and R^2 are shown in Table 4.

The data show that isotherm of dye adsorption onto Cu-NH₂ does not conform the Freundlich and Tempkin isotherms. The R^2 values and the linearity between the C_e/q_e against C_e show that the dye removal isotherm follows Langmuir model (Table 4). This means that the adsorption of dyes takes place at specific homogeneous sites and a one layer adsorption onto adsorbent surface. The maximum adsorption capacity (Q_0) was 227 and 345 mg/g for DR31 and DR80, respectively.

4.7. Kinetic study

Several models can be used to express the mechanism of solute sorption onto a sorbent. In order to investigate the mechanism of sorption, characteristic constants of sorption were determined using pseudo-first-order, pseudo-second-order, and intraparticle diffusion models [37,38].

A linear form of pseudo-first-order model is [37]:

$$\log (q_e - q_t) = \log (q_e) - (k_1/2.303) t \tag{15}$$

where q_t and k_1 are the amount of the adsorbed dye at time t (mg/g) and the equilibrium rate constant of pseudo-first-order kinetics (1/min), respectively.

Table 4

Linearized isotherm coefficients for dye adsorption onto CuO-NH₂ at different adsorbent dosages

Dye	Langmuir				Freundlich			Tempkin		
	Q ₀	K _L	R ²	R _L	K _F	n	R ²	K _T	B ₁	R ²
DR31	227	0.1283	0.8448	0.135	9.9152	5.003	0.4986	7.0435	33.45	0.4649
DR80	345	0.0823	0.9185	0.195	71.845	2.836	0.8861	1.0589	69.63	0.8562

Table 5

Linearized kinetic coefficients for dye adsorption using 50 mg/L of dye at different adsorbent dosages

Adsorbent (g)	(q _e) _{exp}	Pseudo-first-order			Pseudo-second-order			Intraparticle diffusion		
		(q _e) _{cal}	k ₁	R ²	(q _e) _{cal}	k ₂	R ²	k _p	I	R ²
DR31										
0.0125	221	94	0.0539	0.8737	227	0.0018	0.9984	11	138	0.9254
0.0250	162	82	0.0675	0.9342	169	0.0020	0.9993	11	88	0.8988
0.0500	144	84	0.0544	0.8721	149	0.0016	0.9928	10	70	0.9593
0.0750	142	83	0.0716	0.9651	149	0.0002	0.9988	10	73	0.9347
DR80										
0.0250	268	119	0.0468	0.7990	270	0.0005	0.9913	12	166	0.9631
0.0500	236	129	0.0560	0.9422	243	0.0007	0.9958	15	124	0.9921
0.0750	167	98	0.0576	0.9484	175	0.0020	0.9975	12	78	0.9599
0.1000	146	81	0.0532	0.9385	151	0.0038	0.9969	10	70	0.9767

Table 6

Comparison of CuO-NH₂ adsorption capacity among different adsorbents

Adsorbent	Dyes	Adsorption capacity (mg/g)	Concentration (mg/L)	Contact time (h)	Refs.
APTES	RR 3BS	34	120	0.5	[40]
	RB KE-R	38	120	0.5	
MMWCNT	MB	11.8	40	6	[41]
	NR	9.5	40	6	
MnO-Fe ₂ O ₃	AR B	105.5	150	2	[42]
Pd-NPs-AC	CR	76.9	45	0.5	[43]
Ag-NPs-AC	CR	66.7	45	0.5	
ZnO-NRs-AC	CR	142.9	45	0.5	
CuO-NH ₂	DR31	227	50	1	This study
	DR80	345	50	1	

The pseudo-first-order dye removal kinetics was studied by linear plotting of $\log(q_e - q_t)$ against t at different adsorbent dosages and various initial dye concentration in the range of 50–200 mg/L.

Linear form of pseudo-second-order model was illustrated as [37]:

$$t/q_t = 1/k_2 q_e^2 + (1/q_e)t \quad (16)$$

where k_2 is the equilibrium rate constant of pseudo-second-order.

The intraparticle diffusion kinetics of dye adsorption was investigated using the intraparticle diffusion model as [37–39]:

$$q_t = k_p t^{1/2} + I \quad (17)$$

where k_p and I are the intraparticle diffusion rate constant and intercept, respectively.

The kinetics data show that the dye removal can be approximated as pseudo-second-order kinetics

(Table 5). The R^2 values for pseudo-second-order kinetic model were found to be close to 1.0 and the calculated q_e values ($(q_e)_{cal}$) are also very close to that of experimental data ($(q_e)_{exp}$).

4.8. Comparison with other adsorbents

The maximum adsorption capacities (Q_0) were 227 and 345 mg/g for the adsorption of Direct Red 31 and Direct Red 80 respectively. It is obvious that the adsorption capacity of CuO-NH₂ is much better than most of the other functionalized adsorbents reported currently (Table 6) [40–43]. The large values of Q_0 could belong to the adsorption affinity of CuO-NH₂ towards the two dyes, which was caused by the unique surface and charge neutralization.

5. Conclusions

In this paper, the surface functionalized nanoparticle (CuO-NH₂) was synthesized and its dye removal ability was studied. Direct Red 31 (DR31) and Direct Red 80 (DR80) were used as anionic dyes. Dye adsorption capacity of the synthesized adsorbent (CuO-NH₂) for DR31 and DR80 was 227 and 345 mg/g. The Least-squares support vector machine (LSSVM) was used to predict dye removal efficiency. The submitted model shows better performance in predicting dye removal efficiency compared to the kinetic models. Moreover, it was illustrated that the proposed models are capable of simulating the actual physical trend of the dye removal efficiency with variation of adsorbent dosage, initial dye concentration, and initial pH of solution. The results show that the developed model provides predictions in excellent agreement with the experimental data. Furthermore, it is demonstrated that the proposed model is capable of simulating the actual physical trend of the dye removal with alternation of adsorbent dosage, initial concentration of dyes, and initial pH of solution.

References

- [1] N.M. Mahmoodi, Photocatalytic ozonation of dyes using multiwalled carbon nanotube, *J. Mol. Catal. A: Chem.* 366 (2013) 254–260.
- [2] A. Dalvand, M. Gholami, A. Joneidi, N.M. Mahmoodi, Dye removal, energy consumption and operating cost of electrocoagulation of textile wastewater as a clean process, *CLEAN–Soil, Air, Water* 39 (2011) 665–672.
- [3] I.K. Konstantinou, T.A. Albanis, TiO₂-assisted photocatalytic degradation of azo dyes in aqueous solution: Kinetic and mechanistic investigations, *Appl. Catal. B: Environ.* 49 (2004) 1–14.
- [4] N.M. Mahmoodi, N.Y. Limaee, M. Arami, S. Borhany, M. Mohammad-Taheri, Nanophotocatalysis using nanoparticles of titania: Mineralization and finite element modelling of Solophenyl dye decolorization, *J. Photochem. Photobiol. A: Chem.* 189 (2007) 1–6.
- [5] N.M. Mahmoodi, Zinc ferrite nanoparticle as a magnetic catalyst: Synthesis and dye degradation, *Mater. Res. Bull.* 48 (2013) 4255–4260.
- [6] N.M. Mahmoodi, Manganese ferrite nanoparticle: Synthesis, characterization and photocatalytic dyedegradation ability, *Desalin. Water Treat.* 53 (2015) 84–90.
- [7] N.M. Mahmoodi, M. Arabloo, J. Abdi, Laccase immobilized manganese ferrite nanoparticle: Synthesis and LSSVM intelligent modeling of decolorization, *Water Res.* 67 (2014) 216–226.
- [8] N.M. Mahmoodi, M. Arami, F. Mazaheri, S. Rahimi, Degradation of sericin (degumming) of Persian silk by ultrasound and enzymes as a cleaner and environmentally friendly process, *J. Clean. Prod.* 18 (2010) 146–151.
- [9] V. Meshko, L. Markovska, M. Mincheva, A.E. Rodrigues, Adsorption of basic dyes on granular activated carbon and natural zeolite, *Water Res.* 35 (2001) 3357–3366.
- [10] N. Kannan, M.M. Sundaram, Kinetics and mechanism of removal of methylene blue by adsorption on various carbons—A comparative study, *Dyes Pigm.* 51 (2001) 25–40.
- [11] J.A.K. Suykens, J. Vandewalle, Least squares support vector machine classifiers, *Neural Process. Lett.* 9 (1999) 293–300.
- [12] B. Li, Y. Wang, Facile synthesis and photocatalytic activity of ZnO–CuO nanocomposite, *Superlattices Microstruct.* 47 (2010) 615–623.
- [13] A. Eslamimanesh, F. Gharagheizi, M. Illbeigi, A.H. Mohammadi, A. Fazlali, D. Richon, Phase equilibrium modeling of clathrate hydrates of methane, carbon dioxide, nitrogen, and hydrogen + water soluble organic promoters using support vector machine algorithm, *Fluid Phase Equilib.* 316 (2012) 34–45.
- [14] J. Abdi, D. Bastani, J. Abdi, N.M. Mahmoodi, A. Shokrollahi, A.H. Mohammadi, Assessment of competitive dye removal using a reliable method, *J. Environ. Chem. Eng.* 2 (2014) 1672–1683.
- [15] A. Baylar, D. Hanbay, M. Batan, Application of least square support vector machines in the prediction of aeration performance of plunging overfall jets from weirs, *Expert Syst. Appl.* 36 (2009) 8368–8374.
- [16] J.A.K. Suykens, J. De Brabanter, L. Lukas, J. Vandewalle, Weighted least squares support vector machines: Robustness and sparse approximation, *Neurocomputing* 48 (2002) 85–105.
- [17] A. Eslamimanesh, F. Gharagheizi, A.H. Mohammadi, D. Richon, M. Illbeigi, A. Fazlali, A.A. Forghani, M. Yazdizadeh, Phase equilibrium modeling of structure H clathrate hydrates of methane + water “insoluble” hydrocarbon promoter using group contribution-support vector machine technique, *Ind. Eng. Chem. Res.* 50 (2011) 12807–12814.
- [18] C.J. Burges, A tutorial on support vector machines for pattern recognition, *Data Min. Knowl. Discovery* 2 (1998) 121–167.
- [19] A. Chamkalani, A.H. Mohammadi, A. Eslamimanesh, F. Gharagheizi, D. Richon, Diagnosis of asphaltene stability in crude oil through “two parameters” SVM model, *Chem. Eng. Sci.* 81 (2012) 202–208.

- [20] H. Liu, X. Yao, R. Zhang, M. Liu, Z. Hu, B. Fan, Accurate quantitative structure–property relationship model to predict the solubility of C60 in various solvents based on a novel approach using a least-squares support vector machine, *J. Phys. Chem. B* 109 (2005) 20565–20571.
- [21] F. Gharagheizi, A. Eslamimanesh, F. Farjood, A.H. Mohammadi, D. Richon, Solubility parameters of non-electrolyte organic compounds: Determination using quantitative structure–property relationship strategy, *Ind. Eng. Chem. Res.* 50 (2011) 11382–11395.
- [22] A. Eslamimanesh, F. Gharagheizi, A.H. Mohammadi, D. Richon, Phase equilibrium modeling of structure H clathrate hydrates of methane + water “insoluble” hydrocarbon promoter using QSPR molecular approach, *J. Chem. Eng. Data* 56 (2011) 3775–3793.
- [23] D.L. Pavia, G.M. Lampman, G.S. Kaiz, Introduction to Spectroscopy: A Guide for Students of Organic Chemistry, W.B Saunders Company, New York, NY, 1987.
- [24] P. Laokul, V. Amornkitbamrung, S. Seraphin, S. Maensiri, Characterization and magnetic properties of nanocrystalline CuFe_2O_4 , NiFe_2O_4 , ZnFe_2O_4 powders prepared by the Aloe vera extract solution, *Curr. Appl. Phys.* 11 (2011) 101–108.
- [25] S. Xavier-de-Souza, J.A.K. Suykens, J. Vandewalle, D. Bolle, Coupled simulated annealing, *IEEE Trans. Syst. Man Cybern. Part B (Cybernetics)* 40 (2010) 320–335.
- [26] N.M. Mahmoodi, Synthesis of amine-functionalized magnetic ferrite nanoparticle and its dye removal ability, *J. Environ. Eng.* 139 (2013) 1382–1390.
- [27] N.M. Mahmoodi, Surface modification of magnetic nanoparticle and dye removal from ternary systems, *J. Ind. Eng. Chem.* 27 (2015) 251–259.
- [28] N.M. Mahmoodi, B. Hayati, M. Arami, H. Bahrami, Preparation, characterization and dye adsorption properties of biocompatible composite (alginate/titania nanoparticle), *Desalination* 275 (2011) 93–101.
- [29] N.M. Mahmoodi, Synthesis of core-shell magnetic adsorbent nanoparticle and selectivity analysis for binary system dye removal, *J. Ind. Eng. Chem.* 20 (2014) 2050–2058.
- [30] N.M. Mahmoodi, J. Abdi, D. Bastani, Direct dyes removal using modified magnetic ferrite nanoparticle, *J. Environ. Health Sci. Eng.* 12 (2014) 1–10.
- [31] N.K. Amin, Removal of reactive dye from aqueous solutions by adsorption onto activated carbons prepared from sugarcane bagasse pith, *Desalination* 223 (2008) 152–161.
- [32] N.M. Mahmoodi, O. Masrouri, Cationic dye removal ability from multicomponent system by magnetic carbon nanotube, *J. Solution Chem.* 44 (2015) 1568–1583.
- [33] I. Langmuir, The constitution and fundamental properties of solids and liquids. II. Liquids. 1, *J. Am. Chem. Soc.* 39 (1917) 1848–1906.
- [34] I. Langmuir, The adsorption of gases on plane surfaces of glass, mica and platinum, *J. Am. Chem. Soc.* 40 (1918) 1361–1403.
- [35] N.M. Mahmoodi, Dendrimer functionalized nanoarchitecture: Synthesis and binary system dye removal, *J. Taiwan Inst. Chem. Eng.* 45 (2014) 2008–2020.
- [36] Y. Kim, C. Kim, I. Choi, S. Rengaraj, J. Yi, Arsenic removal using mesoporous alumina prepared via a templating method, *Environ. Sci. Technol.* 38 (2004) 924–931.
- [37] N.M. Mahmoodi, O. Masrouri, A.M. Arabi, Synthesis of porous adsorbent using microwave assisted combustion method and dye removal, *J. Alloy. Compd.* 602 (2014) 210–220.
- [38] W. Weber, J. Morris, Kinetics of adsorption on carbon from solution, *J. Sanit. Eng. Div. Am. Soc. Civ. Eng.* 89 (1963) 31–60.
- [39] M. Maghsoudi, M. Ghaedi, A. Zinali, A.M. Ghaedi, M.H. Habibi, Artificial neural network (ANN) method for modeling of sunset yellow dye adsorption using zinc oxide nanorods loaded on activated carbon: Kinetic and isotherm study, *Spectrochim. Acta Part A: Mol. Biomol. Spectrosc.* 134 (2015) 1–9.
- [40] A. Xue, S. Zhou, Y. Zhao, X. Lu, P. Han, Adsorption of reactive dyes from aqueous solution by silylated palygorskite, *Appl. Clay Sci.* 48 (2010) 638–640.
- [41] J.-L. Gong, B. Wang, G.-M. Zeng, C.-P. Yang, C.-G. Niu, Q.-Y. Niu, W.-J. Zhou, Y. Liang, Removal of cationic dyes from aqueous solution using magnetic multi-wall carbon nanotube nanocomposite as adsorbent, *J. Hazard. Mater.* 164 (2009) 1517–1522.
- [42] R. Wu, J. Qu, Y. Chen, Magnetic powder $\text{MnO-Fe}_2\text{O}_3$ composite—A novel material for the removal of azo-dye from water, *Water Res.* 39 (2005) 630–638.
- [43] M. Ghaedi, M.N. Biyareh, S.N. Kokhdan, S. Shamsaldini, R. Sahraei, A. Daneshfar, S. Shahriyar, Comparison of the efficiency of palladium and silver nanoparticles loaded on activated carbon and zinc oxide nanorods loaded on activated carbon as new adsorbents for removal of Congo red from aqueous solution: Kinetic and isotherm study, *Mater. Sci. Eng. C* 32 (2012) 725–734.